Physica Medica 141 (2026) 105698

Contents lists available at ScienceDirect

Physica Medica

journal homepage: www.elsevier.com/locate/ejmp

Original paper

Determining optimal spot delivery pattern using log file Derived dose discrepancy factor in pencil beam scanning reference dosimetry

Kah Seng Lew [a,b,1], Calvin Wei Yang Koh [a], Kang Hao Lee [a], Clifford Ghee Ann Chua [a,b], Andrew Wibawa [a], Zubin Master [a], Wen Siang Lew [b], James Cheow Lei Lee [a,b], Sung Yong Park [a,c], Hong Qi Tan [a,b,c,*]

[a] Division of Radiation Oncology, National Cancer Centre Singapore, Singapore
[b] Division of Physics and Applied Physics, Nanyang Technological University, Singapore
[c] Oncology Academic Clinical Programme, Duke-NUS Medical School, Singapore

A B S T R A C T

Introduction: Spatial uncertainties in spot position during reference dosimetry measurements of pencil beam scanning system were found to cause fluctuations in the reference dosimetry curve. This study aims to develop a method to determine the optimal delivery pattern for reference dosimetry measurement using information obtained from log file and quantifying the expected dose discrepancy.

Methods: A total of 7 different delivery pattern were delivered five times each and log files for each delivery were collected. We introduced a new metric known as dose discrepancy factor (DDF) to quantify the expected dose discrepancy in the measurement arising from spot positioning error. DDF is calculated using a simple pencil beam algorithm and actual spot positions from the log file. Type A and B uncertainties of DDF are quantified to draw statistically rigorous conclusion on the most optimal delivery pattern.

Results: Relative dose difference of up to 2 % can be observed in some of the delivery pattern when reference dosimetry curve was plotted. Linear fit of DDF calculated from log file against measured dose ratio yields an R^2 of 0.56 which suggest moderate correlation. Delivery patterns with repainting and X fast scan (50MU) have the lowest average uncertainty. Friedman test and post-hoc test shows that different delivery patterns were proven to be statistical different with the exception of Y fast scan (50MU) versus both X fast scan (50MU) and random scan (50MU). Y fast scan (50MU) with the highest average DDF value of 0.979 ± 0.005 was found to be the most optimal delivery pattern as it has the least discrepancy from an ideal delivery.

Conclusion: Delivery patterns used during reference dosimetry had a non-negligible impact on measurement. We had detailed a log file-based approach to determine the optimal delivery pattern such that dose measurement would be least affected by spot positioning error.

1. Introduction

Proton therapy has been shown to be more beneficial compared to conventional X-ray therapy as it reduces the radiation dose to normal tissue while providing the radiation dose required to the tumour [1–5]. Protons exhibits a distinct Bragg peak which has minimal exit dose and while depositing most of their energy at the end of range [6]. This unique property provides superior normal tissue sparing, as the dose can be precisely modulated to deposit most of the radiation within the tumour [7]. Pencil beam scanning (PBS) delivery system is a technique that delivers small proton beamlets by magnetically scanning them across the tumour using two pairs of scanning magnets [8,9]. By systematically changing the energy of the protons, we can precisely control the depth of proton penetration within the tissue allowing for three-dimensional dose painting that conforms to the tumour's volume [10,11]. Because of the increasing clinical evidence showing that PBS delivery system being more beneficial than passive scattering, it is increasingly being used in intensity modulated proton therapy (IMPT) and older facilities are upgrading from passive scattering to pencil beam scanning [12–14].

In the commissioning of a PBS treatment planning system (TPS), reference dosimetry data is instrumental in defining the number of proton particles per monitor units (MU) for the TPS to arrive at an accurate dose. The reference dosimetry measurement can be related mathematically to the measurement of the integrated absorbed dose to water, also known as the dose area product (DAP_w) [15,16]. By scaling DAP_w using CEMA (converted energy per unit mass), DAP_w can be related to the number of protons per monitor units (MU) for a particular

* Corresponding author at: Division of Radiation Oncology, National Cancer Centre Singapore, Singapore.
E-mail address: tan.hong.qi@nccs.com.sg (H.Q. Tan).
[1] First authors.

https://doi.org/10.1016/j.ejmp.2025.105698
Received 17 March 2025; Received in revised form 5 August 2025; Accepted 11 December 2025
Available online 13 December 2025
1120-1797/© 2025 Associazione Italiana di Fisica Medica e Sanitaria. Published by Elsevier Ltd. All rights are reserved, including those for text and data mining, AI training, and similar technologies.

energy [16–18]. In the latest revision of TRS 398, the reference conditions of reference dosimetry in PBS delivery system are included which consists of the use of a uniformly single-layer scanned field large enough to achieve lateral charged particle equilibrium [19]. However, because of stochastic intra-spill spot drift, consistent reference dosimetry measurement is a challenge during repeated measurement. This has been documented in detail in the study by H. Q. Tan et al [20]. These spot positional uncertainties can potentially cause errors that propagate through to the dose received by the patient [21]. Firstly, dose calculation accuracy within the TPS is affected as beam modelling is inaccurate due to systematic errors being introduced in the protons per MU definitions in the TPS, resulting in misrepresentation of the actual dose distribution. Secondly, the spot positional drift during the actual treatment also introduces another layer of errors as the intended dose distribution might be affected [22,23].

In this study, we first show the choice of spot delivery patterns for reference dosimetry can lead to different measurement results due to different spot positional deviation distributions. In light of this, we aim to develop a method to determine the optimal delivery pattern for reference dosimetry to reduce the effect of spot positional drift on the final measurement. We introduce a dose discrepancy factor (DDF) which is calculated from the log file of the delivery to quantify the expected dose discrepancy in the reference dosimetry measurement arising from spot position errors. The type A and B uncertainties of DDFs are also quantified to ensure that the DDFs calculated for seven unique delivery patterns can be distinguished in a statistically rigorous manner.

2. Methodology

2.1. Delivery conditions and log file

In National Cancer Centre Singapore (NCCS), the Hitachi Probeat proton therapy system has a synchrotron accelerator that is capable of delivering 98 discrete energies from 70.2 MeV to 228.7 MeV. This corresponds to a beam range (R_{90}) of 3.9 cm to 32.9 cm in water with R_{90} defined as 90 % of the dose level in the distal end of the Bragg peak. The system has a spot sigma ranging from 1.9 mm to 5.6 mm in air when measured at isocentre (770 mm from the vacuum window) and has a minimum monitor unit (MU) of 0.003 and a maximum MU of 0.2. Inside the treatment nozzle as seen in the schematic in Fig. 1a, treatment delivery is monitored by the spot position monitor (SPM), main dose monitor (DM1) and sub dose monitor (DM2). After every delivery, the data from the SPM and DMs were recorded in log files which contain the following information for each delivered spot: 1) actual MU delivered (recorded by DM1 and DM2), 2) X and Y spot position, 3) X and Y spot width. In each log file, together with the X and Y spot position were the raw data that were used to determine the position of each spot. The SPM consisted of 300 electrode wires in the X direction and 440 electrode wires in the Y direction with a pitch of 0.8 mm. A channel data analysis was then performed as illustrated in Fig. 1b where Gaussian fitting was used to determine the position of each spot.

To study the impact of delivery patterns on reference dosimetry measurement, 10 different energies (70.2 MeV, 81.8 MeV, 94.6 MeV, 116.4 MeV, 142.4 MeV, 150.2 MeV, 168.0 MeV, 187.5 MeV, 208.3 MeV and 228.7 MeV) were delivered and the charges were measured using a PTW 34045 (Advanced Markus Chamber) ionisation chamber. Following the reference conditions recommended in the revised TRS-398, a 10 x 10 cm^2 square field with a spot spacing of 2.5 mm was delivered and the ionisation chamber was placed at a fixed measurement depth of 2 cm in water. A total of seven different delivery patterns were delivered:

1. Y fast scan (8 MU)
2. Y fast scan (50 MU)
3. X fast scan (8 MU)
4. X fast scan (50 MU)

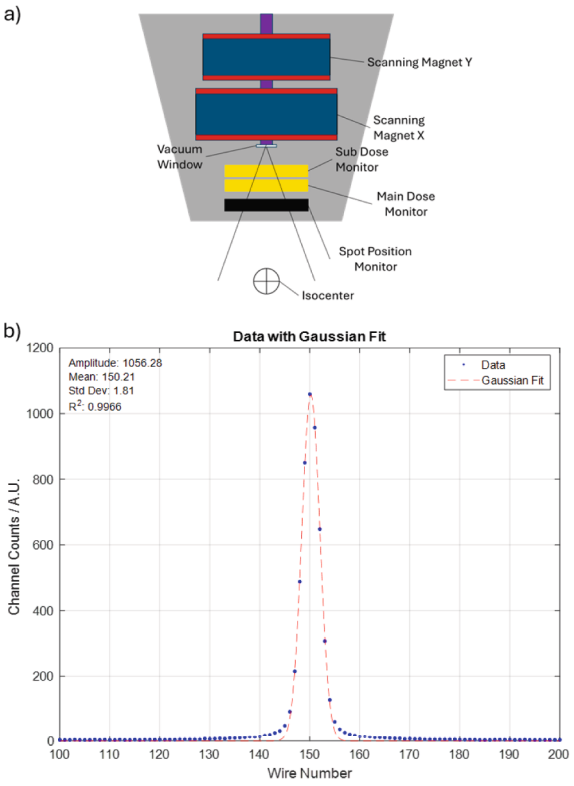

Fig. 1. Schematic of Hitachi's scanning nozzle and channel data analysis of raw log file data. a) This figure shows a schematic of the scanning magnets, dose monitors and spot position monitor inside the scanning nozzle of Hitachi's Probeat proton therapy machine. b) This figure shows the Gaussian fit used to determine the position of a spot using the raw data found inside the log file.

5. Y fast scan 3 repainting (50 MU)
6. Y fast scan 5 repainting (50 MU)
7. Random scan (50 MU).

Fast scan was defined as the direction in which the beam was delivered first in a serpentine manner. Each of the delivery patterns were irradiated five times and the delivery log files were collected after each delivery. Following the formalism in IAEA TRS-398, absorbed dose to water in reference conditions for proton beams was corrected for all influence quantities and the absorbed dose across different delivery patterns was measured.

2.2. Dose discrepancy factor and regression analysis

In this work, we introduced the dose discrepancy factor (DDF) to quantify the expected discrepancy in the measured dose using the log file parameters. It is defined as:

$$DDF = \frac{D(x,y,z;E)_{Delivered}}{D(x,y,z;E)_{Ideal}}, \quad (1)$$

where $D(x,y,z;E)_{Delivered}$ is the delivered dose calculated using actual delivered spot parameters in the log files and $D(x,y,z;E)_{Ideal}$ is the dose calculated using actual delivered spot parameters in the log files with the exception that the spot position is replaced by the planned delivery position. A simplified pencil beam algorithm was developed using MATLAB (version R2024a, The MathWorks Inc, Natick, Massachusetts) for dose calculation by considering only the integrated dose over the detector's sensitive volume from a single energy layer delivery in a homogenous water medium:

$$D(x,y,z;E) = \sum_{i=1}^{N} \frac{IDD(z)}{IDD(2cm)} \times G\left[x,y;\mu_{x,i}(z),\mu_{y,i}(z),\sigma_{x,i}(z)\times\sigma_{y,i}(z)\right] \times MU_i \times C(E). \quad (2)$$

x And y were the spot positions with respect to the isocentre, z was the depth from the surface of the medium, $IDD(z)$ was the integrated depth dose curve at depth z and $G\left[x,y;\mu_{x,i}(z),\mu_{y,i}(z),\sigma_{x,i}(z)\times\sigma_{y,i}(z)\right]$ was the 2D Gaussian representation of a single spot with $\mu_{x,i}(z)$ and $\sigma_{x,i}(z)$ representing the position of the spot centroid and spot sigma respectively at depth z. MU_i was the MU delivered for spot i and $C(E)$ was the calibration factor in cGy/MU of each energy layer. Intuitively, the dose discrepancy factor *is used to quantify the error in the measured dose due to spot positioning error*. For instance, a factor closer to 1 represents that the measured dose is free of the influence of spot positioning error while, $DDF \gg 1$ or $DDF \ll 1$ implies that the measured dose might not be reliable

By manipulating **Eqn (1)**, we arrived at

$$DDF_{ref} = \frac{DDF}{DDF_{Yfastscan,50MU}} = \frac{D(x,y,z;E)_{Delivered}}{D(x,y,z;E)_{Yfastscan,50MU}}. \quad (3)$$

$D(x,y,z;E)_{Yfastscan,50MU}$ was chosen arbitrability as the reference delivery. Practically, the estimated dose ratio calculated from log file, DDF_{ref}, should be equal to the measured dose ratio up to a linear and constant difference due to measurement noise and different sensitivities. Hence, denoting $D^{meas}(x,y,z;E)$ as the measured dose, we obtained

$$DDF = k \times \frac{D^{meas}(x,y,z;E)_{Delivered}}{D^{meas}(x,y,z;E)_{Yfastscan,50MU}} + \epsilon. \quad (4)$$

From **Eqn (4)**, a regression analysis between the calculated DDF_{ref} from log file and the measured $\frac{D^{meas}(x,y,z;E)_{Delivered}}{D^{meas}(x,y,z;E)_{Yfastscan,50MU}}$ should yield a straight line. This will be used to establish if the use of DDF_{ref} was representative of the dose discrepancy measured by the ionisation chamber. DDF_{ref} was calculated for all the remaining 30 deliveries (6 other unique patterns x 5 repetitions) and all the data was included in the regression analysis. Regression analysis was chosen to test for the monotonic relationship between the two variables where R^2 shows the variance explained by the linear fit.

2.3. Type A and type B uncertainty analysis of the DDF

The type A and B uncertainties of the DDF were defined and quantified in this study. This is important so that statistically meaningful conclusions can be drawn when comparing the *DDFs* between different deliveries to arrive at the "best" delivery pattern with the least discrepancy arising from spot delivery error. Two type A uncertainties were identified during the computation of *DDF*. The first uncertainty arises from the repeatability of the spot exiting the nozzle; it is not possible for the spot to be incident on the same coordinate (x,y) in every delivery. The second uncertainty is due to the statistical error in the recorded spot position in the log file due to Gaussian fitting to the raw signal in the SPM. To quantify these two errors together, the detailed log files (containing the counts in every channel in the SPM) for the five repeated measurements of each delivery were extracted. Using the raw data of each log file, X and Y spot channel data were fitted with a Gaussian function to calculate the 1σ confidence interval for each of the X and Y spot positions. The X and Y spot positions in each delivery were sampled 50 times (bootstrapping) from this confidence interval for each spot to account for fitting uncertainties. By applying this process to the five repeated deliveries, both uncertainties were taken into account, and this resulted in a total of 250 *DDFs*. The standard deviation was calculated from the 250 *DDFs* to represent the type A uncertainty for each energy and delivery pattern.

There were several sources of type B uncertainties in this study. However, we focused only on the SPM specific uncertainty which was the systematic offset in the wires arising from the misalignment of the SPM. A systematic offset of 0.5 mm and 1.0 mm was introduced in the X position, Y position and both X and Y positions of each ideal delivery. A maximum shift of 1.0 mm was used as the spot position tolerance due to the daily, monthly and annual QA tolerance in TG-224 [24]. From the log files, the offsets were added to the planned spot position for dose calculation using **Eqn (2)**. We then calculated the *DDF* of each energy in all the delivery patterns for the spot positions with the offsets. The type B uncertainty was then quantified from the difference between the *DDFs* calculated with and without the offsets. Finally, as both type A and type B uncertainty were independent sources of uncertainty the combined uncertainty can be added in quadrature using the following formula:

$$\sigma_{A+B} = \sqrt{\sigma_A^2 + \sigma_B^2}, \quad (5)$$

where σ_A and σ_B were the type A and type B uncertainty respectively.

With the calculated combined type A and B uncertainties, we used the Friedman test to test the null hypothesis that there was no difference between the different delivery patterns. A two-tailed $P < 0.05$ was considered statistically significant in this study. If $P < 0.05$ was obtained for Friedman test, Nemenyi post-hoc test was then used to conduct pairwise test on the different delivery pattern pairs. This would allow us to conclude if there was any statistically significant difference between any two delivery patterns.

3. Results

3.1. Corrected absolute dose measurement for different delivery pattern

The dose measurements results of all the delivery patterns and for all the 10 proton energies are shown in In Fig. 2a. The error bars in the figure represented the 1σ error arising from repeatability of measurement. In Fig. 2b, the percentage difference relative to the average dose of each energy is plotted. When comparing across all energies and delivery patterns, a maximum relative difference of 1.9 % was obtained for Y fast scan with 3 repainting (50 MU) for 208.3 MeV. Comparing across the different delivery pattern, X fast scan (8 MU) had the largest mean absolute error of (0.5 ± 0.2) % while comparing across the energies, 228.7 MeV had the largest mean absolute error of (0.7 ± 0.5) %. The detailed plots of X and Y spot positions of a single delivery for all the different delivery patterns can be found in **Fig. S1**.

3.2. Dose discrepancy factor and regression analysis

The linear fit performed using DDF_{ref} and dose normalised to reference delivery as stated in **Eqn (3)** is plotted in Fig. 3. A prediction bound of 90 % is also plotted with those falling outside of the bound treated as an outlier. A total of 5 points were treated as outliers during fitting and the final plot of the fit with all the points and the new prediction bound is shown in Fig. 3. Overall, a R^2 of 0.56 was obtained showing that DDF_{ref} was moderately correlated to the measured dose ratio.

3.3. Type A and type B uncertainty of DDF

In Fig. 4, the calculated uncertainties for delivery patterns: a) Y fast scan (50 MU), b) Y fast scan (8 MU), c) random scan (50 MU), d) Y fast scan with 3 painting, e) Y fast scan with 5 painting, f) X fast scan (50 MU), and g) X fast scan (8 MU) are plotted using bar charts. Across all the 7 plots, we could see that type A uncertainties contributed a larger part of the combined uncertainty. For type B uncertainty, a larger offset resulted in a larger uncertainty which was expected. Also, type B uncertainty generally had a larger impact on the higher energies as compared to the lower energies regardless of delivery patterns. Comparing 50 MU and 8 MU delivery for both X fast scan and Y fast scan,

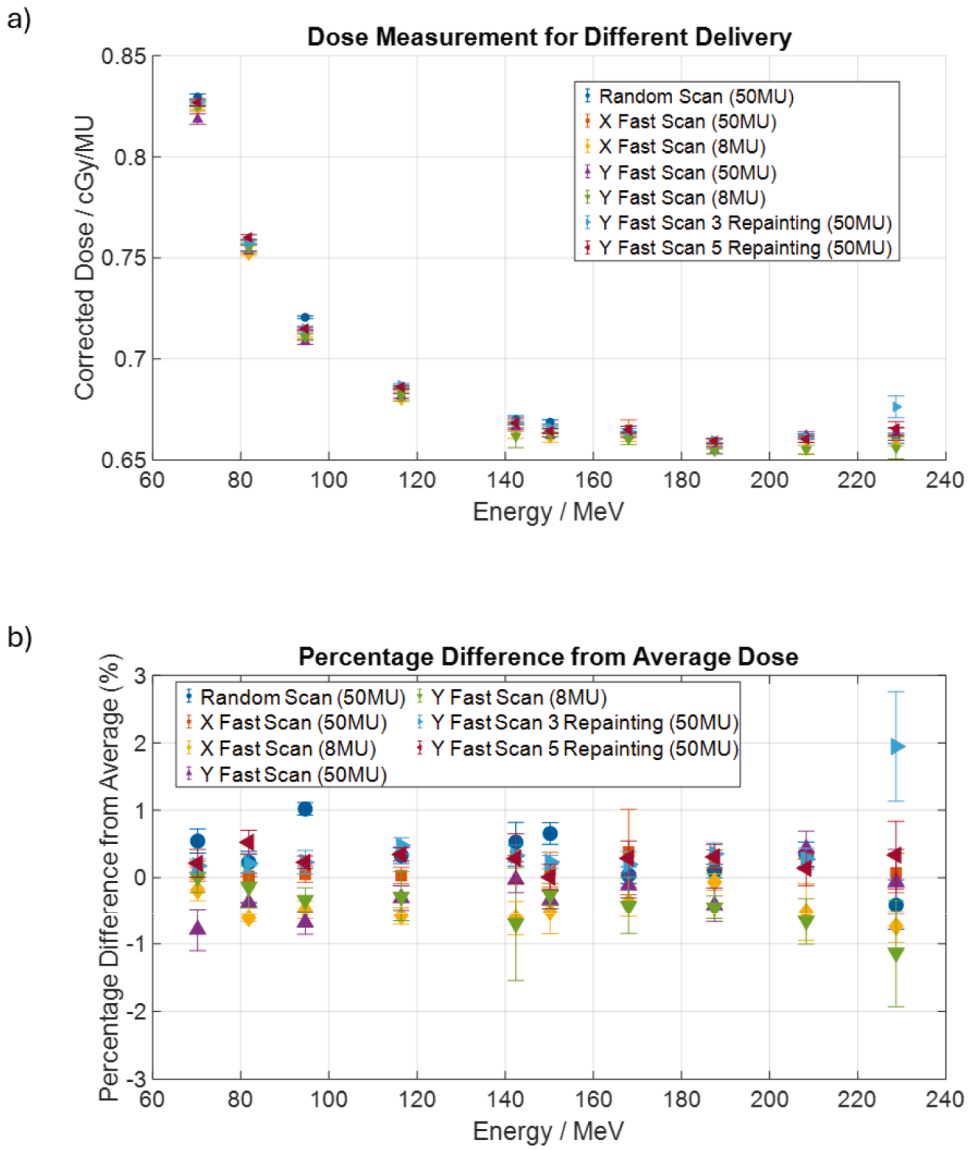

Fig. 2. Advanced Markus ionisation chamber measurements for different delivery patterns and the relative variation from average. a) This figure shows the reference dosimetry measurement across the different delivery patterns as indicated by the different shape markers. b) This figure shows the percentage deviations of different delivery pattern measurement from the average values.

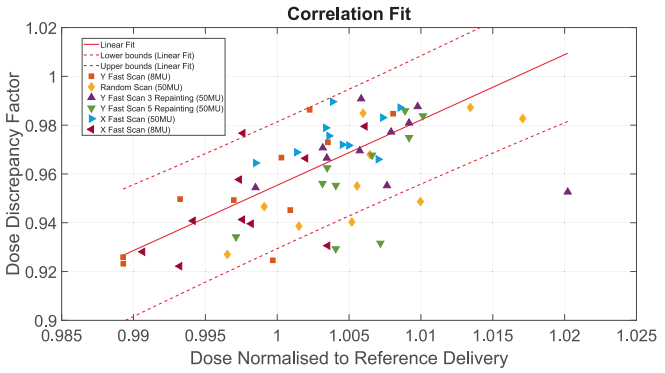

Fig. 3. Linear fit between DDF and dose normalised to reference delivery (Y fast scan (50 MU)). This figure shows the linear fit obtained from DDF and dose normalised to reference delivery. The different marker shows the different delivery pattern while the dotted line shows the prediction bound for the linear fit.

we could see that delivery patterns with 8 MU had a larger type B uncertainty. Among all the different delivery pattern, Y fast scan with 5 repainting (50 MU) had the lowest uncertainty. In Fig. 4a and Fig. 4**c, 187.5** MeV has the highest uncertainty while Fig. 4b, Fig. 4d and Fig. 4f has the highest uncertainty at 228.7 MeV. Lastly, Fig. 4g has the highest uncertainty at 208.3 MeV.

In Fig. 5a and Fig. 5b, *DDF* was plotted together with the combined type A and B uncertainties that were calculated in the previous part. Fig. 5a and Fig. 5b were found to have largely similar trends with 1.0 mm offset having a slightly larger uncertainty as compared to 0.5 mm offset. Corresponding the plot of Fig. 5b to Table 1, the largest *DDF* was found at X fast scan (8MU) for 228.7 MeV with a value of 0.991 ± 0.001 while the smallest *DDF* of 0.922 ± 0.007 was found at Y fast scan with 3 repainting (50 MU) for 81.8 MeV.

A Friedman test was performed to analyse differences between delivery patterns. The test yielded a significant result ($P < 0.01$) for the paired group comparison. The subsequent Nemenyi post-hoc test results are visualized in Fig. 6. All pairwise comparisons showed significant differences ($P < 0.05$) except for two pairs: the Y fast scan (50 MU)

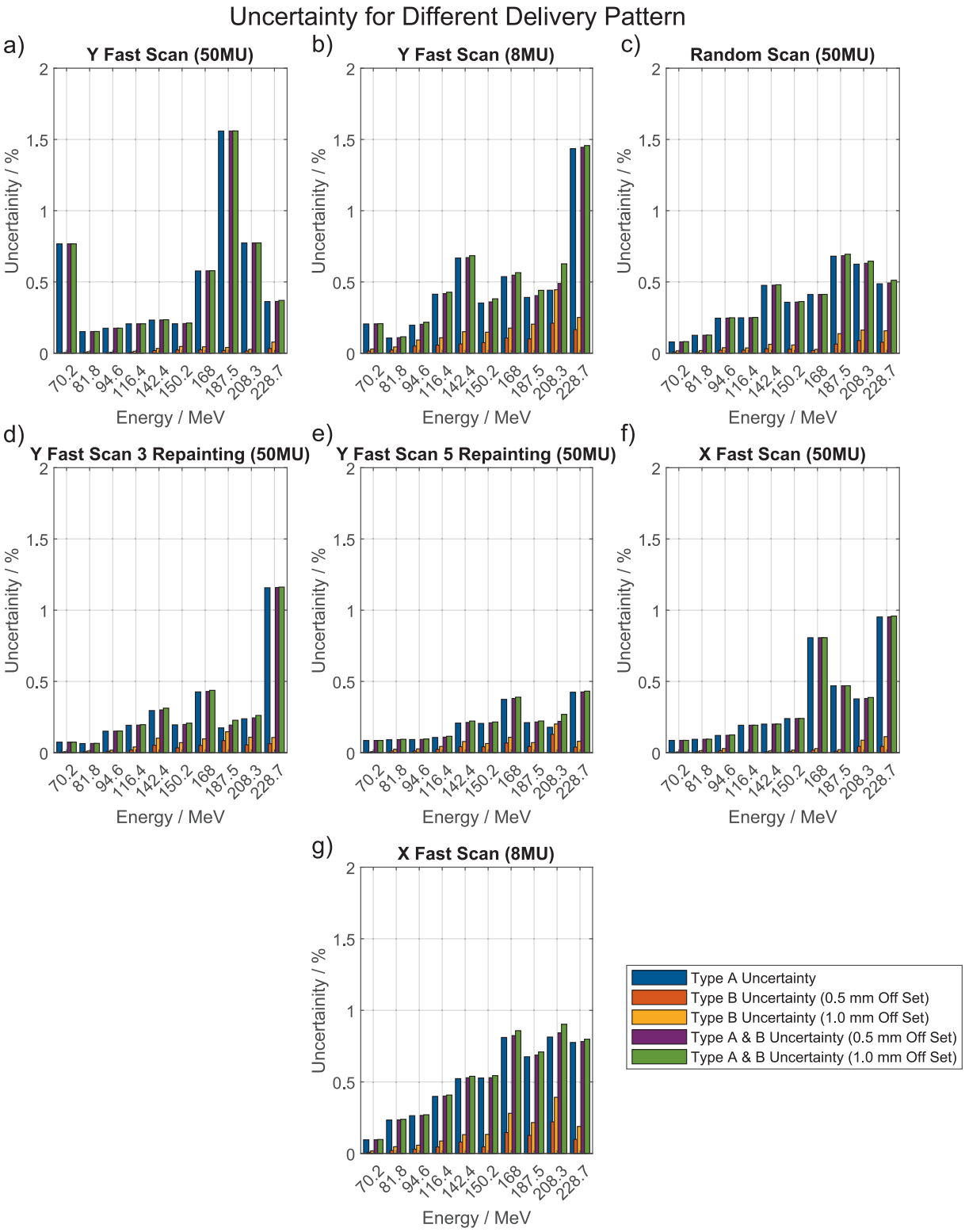

Fig. 4. Calculated uncertainty for different delivery pattern. This figure shows the type A uncertainty, type B uncertainty (0.5 mm offset and 1.0 mm offset), combined uncertainty (0.5 mm offset) and combined uncertainty (1.0 mm offset) for a) Y fast scan (50 MU), b) Y fast scan (8 MU), c) random scan (50 MU), d) Y fast scan with 3 painting, e) Y fast scan with 5 painting, f) X fast scan (50 MU), and g) X fast scan (8 MU).

versus X fast scan (50 MU), and the Y fast scan with 5 repainting (50 MU) versus random scan (50 MU). These results led to the rejection of the null hypothesis, indicating significant differences exist between most delivery patterns.

4. Discussion

In this work, we first investigated how different delivery patterns could affect the absolute dose measurement. In TG-224, output constancy tolerance was recommended to be ± 2 %, however Fig. 2b

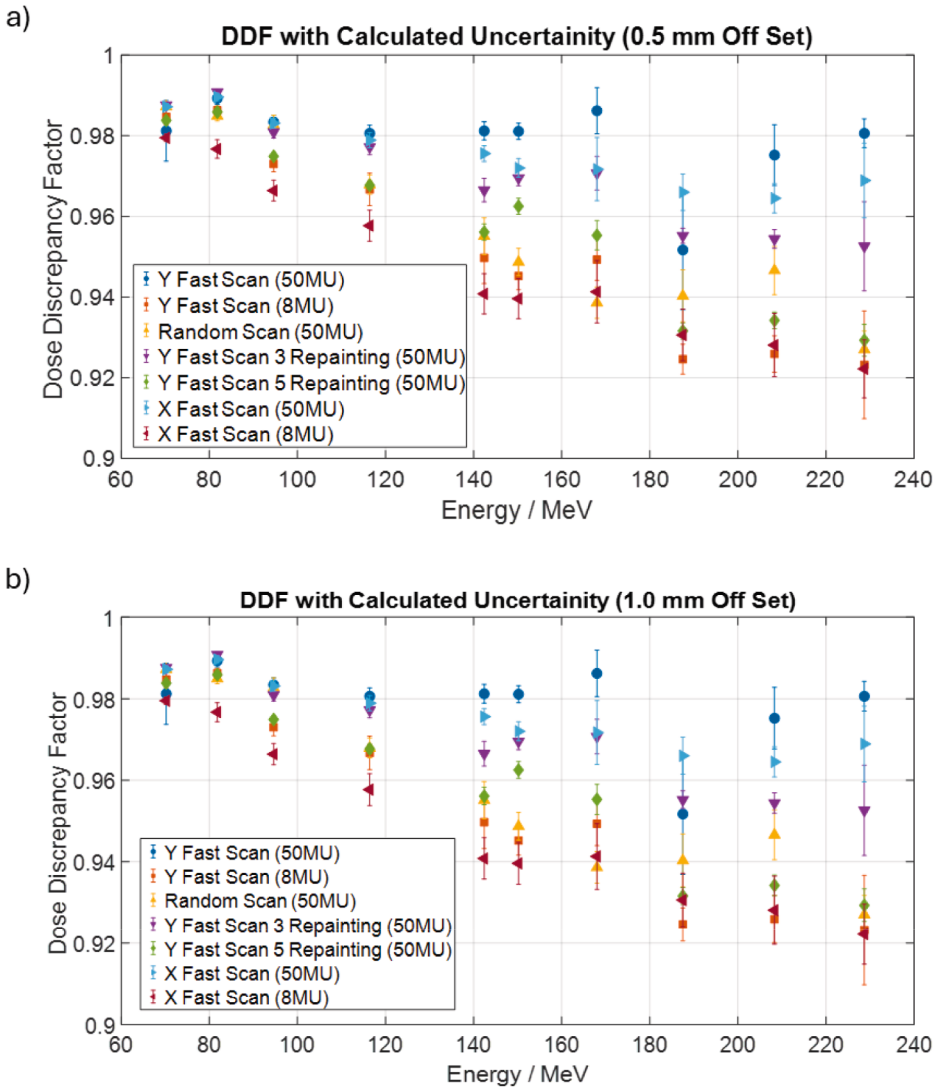

Fig. 5. DDF and overall type A and type B uncertainty. a) DDF with calculated type A uncertainty and type B uncertainty (0.5 mm offset) for all delivery patterns plotted together. b) DDF with calculated type A uncertainty and type B uncertainty (1.0 mm offset) for all delivery patterns plotted together.

showed that there were some measurements having a difference close to this tolerance. This observation is consistent with the report by H. Q. Tan et al., where they had previously shown that spot position played a significant role in the reliable measurement of dose with ionisation chamber [20,24]. Across all the delivery patterns, the maximum absolute spot position errors are 0.75 mm and 0.58 mm respectively for X and Y spot position. These values are within the interlock set by the vendor which is ± 1 mm.

DDF was quantified for all the 35 deliveries and the results were summarised in Table 1. DDF_{ref} was plotted against the normalized absorbed dose in Fig. 3 and a linear regression fit was performed according to **Eqn (5)**. Even though the R^2 was modest with a value of 0.56, it does show that *DDF* was correlated to the dose difference between deliveries. The unexplained variance in the linear regression could be attributed to the dose measurement uncertainty and the spot position related type A and B uncertainties.

During the quantification of the type A and B uncertainties of the *DDF*, we found that type A uncertainties constituted the majority of the overall uncertainty as compared to type B uncertainty. Type A uncertainty consisted of random spot positioning errors that could cause hot and cold spots in the field. This would affect the dose measurement if the hot and cold spots occurred near the ionisation chamber. On the other hand, the type B uncertainty due to the SPM systematic offset was less significant if the field was flat (devoid of spot positioning errors). This was observed in our study when the offset was introduced in an ideal delivery where the planned spot positions were used to compute the *DDF*. Overall, Y fast scan with 5 repainting (50 MU) had the lowest combined uncertainty. This was expected as the averaging effect of repainting would help to reduce the hot and cold spots. Another observation was also that when comparing Fig. 4a, Fig. 4d and Fig. 4e, the type B uncertainty increased with increasing repainting. This increase in type B uncertainty could also be observed when the MU was reduced from 50 MU to 8 MU as seen in Fig. 4a, Fig. 4b, Fig. 4f and Fig. 4g. Looking at average *DDF* values in Table 1, Y fast scan (50 MU) and both deliveries with 8 MU showed the largest average uncertainty across the different delivery patterns.

From Fig. 5, *DDF* was found to decrease with increasing proton energy indicating a larger dose discrepancy at higher energies. These results are consistent with the simulation findings of Yu, Beltran, and Herman's simulation using consistent position error and spot spacing across different energies which suggest that having a smaller spot sigma causes a larger dose discrepancy [22]. Both Fig. 5a and Fig. 5b exhibited a similar uncertainty with type B uncertainty being negligible compared to type A uncertainty. The dose discrepancy was consistently larger for 8

Table 1
This table shows the average DDF values for the five repeated measurements across each delivery pattern and energy. The uncertainties associated with each DDF values are calculated from the type A and type B uncertainties with 1.0 mm offset as shown in Fig. 4. The average DDF of each energy and delivery pattern is also calculated as shown.

Energy	Y Fast Scan (50MU)	Y Fast Scan (8MU)	Random Scan (50MU)	Y Fast Scan 3 Repainting (50MU)	Y Fast Scan 5 Repainting (50MU)	X Fast Scan (50MU)	X Fast Scan (8MU)	Average (Energy)
70.2	0.981 ± 0.008	0.985 ± 0.002	0.987 ± 0.001	0.988 ± 0.001	0.984 ± 0.001	0.987 ± 0.001	0.980 ± 0.001	0.984 ± 0.002
81.8	0.989 ± 0.002	0.986 ± 0.001	0.985 ± 0.001	**0.991 ± 0.001**	0.986 ± 0.001	0.990 ± 0.001	0.977 ± 0.002	0.986 ± 0.001
94.6	0.983 ± 0.002	0.973 ± 0.002	0.983 ± 0.002	0.981 ± 0.001	0.975 ± 0.001	0.983 ± 0.001	0.966 ± 0.003	0.978 ± 0.002
116.4	0.981 ± 0.002	0.967 ± 0.004	0.968 ± 0.002	0.977 ± 0.002	0.968 ± 0.001	0.979 ± 0.002	0.958 ± 0.004	0.971 ± 0.002
142.4	0.981 ± 0.002	0.950 ± 0.006	0.955 ± 0.005	0.967 ± 0.003	0.956 ± 0.002	0.976 ± 0.002	0.941 ± 0.005	0.961 ± 0.004
150.2	0.981 ± 0.002	0.945 ± 0.003	0.949 ± 0.003	0.970 ± 0.002	0.963 ± 0.002	0.972 ± 0.002	0.940 ± 0.005	0.960 ± 0.003
168.0	0.986 ± 0.006	0.949 ± 0.005	0.939 ± 0.004	0.971 ± 0.004	0.955 ± 0.004	0.972 ± 0.008	0.941 ± 0.008	0.959 ± 0.006
187.5	0.952 ± 0.015	0.925 ± 0.004	0.940 ± 0.006	0.955 ± 0.002	0.932 ± 0.002	0.966 ± 0.005	0.931 ± 0.006	0.943 ± 0.0006
208.3	0.975 ± 0.008	0.926 ± 0.006	0.947 ± 0.006	0.954 ± 0.002	0.934 ± 0.002	0.965 ± 0.004	0.928 ± 0.008	0.947 ± 0.005
228.7	0.981 ± 0.004	0.923 ± 0.013	0.927 ± 0.005	0.953 ± 0.0011	0.929 ± 0.004	0.969 ± 0.009	**0.922 ± 0.007**	0.943 ± 0.008
Average (Delivery Patterns)	0.979 ± 0.005	0.953 ± 0.005	0.958 ± 0.004	0.971 ± 0.003	0.958 ± 0.002	0.976 ± 0.003	0.948 ± 0.005	

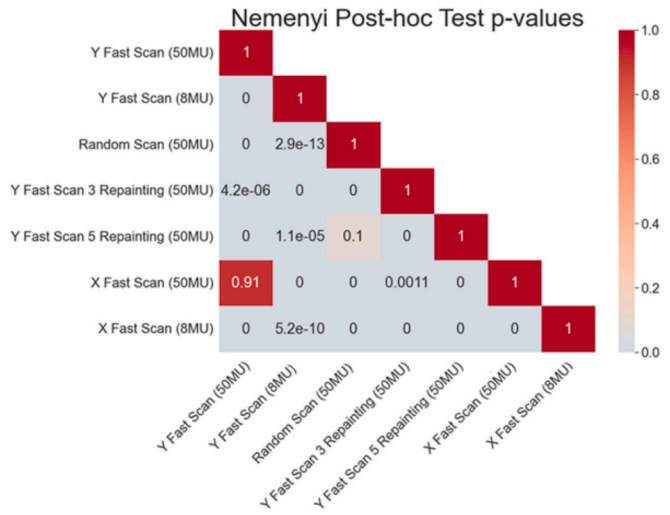

Fig. 6. P-values for different deilvery pattern using Nemenyi's post-hoc test. This figure shows the p-values of all delivery pattern pair when post-hoc test is performed after obtaining p-value of < 0.05 for Friedman test.

MU delivery compared to 50 MU, irrespective of scan direction. However, Y fast scan had a lower dose discrepancy as compared to X fast scan.

As seen in Table 1, Y fast scan with 5 repainting (50MU), Y fast scan with 3 repainting (50 MU) and Y fast scan (50 MU) with no repainting shows a decreasing uncertainty magnitude with increased repainting frequency. This was expected as the repainting helps to average out any hot and cold spots that are formed during delivery providing a more uniform dose distribution. But one should take note that the calculated *DDF* also showed repainting increases the dose discrepancy.

Lastly, the Friedman test showed that there were statistically significant differences between the different deliveries. The ensuing post-hoc test revealed that the X fast scan (50 MU) versus Y fast scan (50 MU), and random scan (50 MU) versus Y fast scan with 5 repainting were the only two comparisons with no significant difference between the deliveries ($P > 0.05$.).

Combining the average *DDF* values and the uncertainties calculated, the most optimal delivery pattern to be used for reference dosimetry measurement was Y fast scan (50 MU). It is also important that during reference dosimetry measurement, care should be taken when changing delivery parameters such as MUs or repainting to minimising dose fluctuation as discrepancy might be introduced in the measured dose as seen in this work. The scanning direction of delivery pattern is also found to have little impact as evident from the small difference in *DDF* values for both X and Y fast scan (50 MU). This is further supported by the *P* value of post-hoc test which show no significant difference. Additional analysis of the delivered spot position for these two deliveries found that for X fast scan (50 MU), the standard deviation for x spot position is 0.16 mm while the y spot position is 0.08 mm. For Y fast scan (50 MU), the standard deviation was 0.17 mm for x spot position and 0.09 mm for y spot position.

One approach to circumventing the impact of spot position errors during reference dosimetry measurements is through the use of large area ionization chambers (LAICs) [18]. These chambers offer larger collection volumes that can accommodate the positional uncertainty of the single spot used during measurements. However, LAICs present a challenge as they typically do not come with calibration factors from accredited dosimetry calibration laboratories and requires us to perform cross calibration against ionisation chamber with traceable calibration factors. This process can be challenging with the detailed methodology for obtaining reliable calibration factors for LAICs in proton beam dosimetry found in multiple papers [15,16,25]. H. Q. Tan et al. also proposed another method for reducing the impact of spot positional errors through smoothing of the reference dosimetry curve [26]. However, this method introduces additional uncertainties associated with the functional fitting process which could potentially impact the overall accuracy of the dosimetry measurements. Therefore, careful evaluation should be performed before implementation. The use of standard test volume (STV) has also been recommended by the Institute of Physics and Engineering in Medicine (IPEM) for reference dosimetry [27]. While this method could potentially reduce the impact of spot positioning errors but the requirement of a monoenergetic energy layer delivery during initial TPS commissioning can still benefit from the methodology in this work. In all, we have we have introduced a method to determine the optimal delivery pattern to be used for reference dosimetry such that the final measurement has minimal impact from spot positioning error.

In this study, only uncertainties relating directly to spot positioning errors were discussed as other inherent uncertainties in the beam delivery system and during measurement remained present but were expected to be relatively constant across measurements. Another potential limitation in this work relates to the quality assurance of the SPM. The accuracy of *DDF* and uncertainty calculations for determining optimal delivery patterns introduced in this work depends on the reliability of the SPM logged data. However, verification of SPM accuracy presents two significant challenges: first, the validation of SPM performance primarily relies on vendor calibration, without independent verification methods readily available to end users. Second, the tools required for validating sub-millimetre spot position accuracy are not commonly accessible in clinical settings. In this case, users can work closely with vendors such that results from their routine maintenance work are made available. As spot sigma and spot deviation profiles are system specific, which can vary between synchrotrons, our optimal delivery pattern may not be directly applicable to other centers. Other centers should instead reproduce this work to determine the optimal delivery pattern for their system for reference dosimetry measurements.

5. Conclusion

In this study, we investigated the impact of different delivery patterns on the reference dosimetry measurements. We also introduced a new metric calculated from the delivery log file, *DDF*, to quantify the degree of dose discrepancy in the measured dose arising from spot position errors. Through the further quantification of the type A and B uncertainties of *DDF*, we further showed that our *DDF* metric could be used to distinguish the expected dose discrepancy between different delivery patterns. Our approach showed that Y fast scan (50 MU) has a *DDF* closest to unity and should be used for reference dosimetry for minimal impact of spot positioning errors on the measured dose. The approach outlined in this work could be used in other clinics when deciding on the optimal delivery pattern to be used for reference dosimetry.

6. Funding support

Hong Qi Tan is supported by the Duke-NUS Oncology Academic Program Goh Foundation Proton Research Programme (08/FY2024/EX (SL)/163-A252).

Declaration of competing interest

The authors declare that they have no known competing financial interests or personal relationships that could have appeared to influence the work reported in this paper.

Appendix A. Supplementary data

Supplementary data to this article can be found online at https://doi.org/10.1016/j.ejmp.2025.105698.

References

[1] Kandula S, et al. Spot-scanning beam proton therapy vs intensity-modulated radiation therapy for ipsilateral head and neck malignancies: a treatment planning comparison. Med Dosim 2013;38:390–4.
[2] Sakthivel V, Ganesh KM, McKenzie C, Boopathy R, Selvaraj J. Second malignant neoplasm risk after craniospinal irradiation in X-ray-based techniques compared to proton therapy. Australas Phys Eng Sci Med 2019;42:201–9.
[3] Simone CB, Rengan R. The use of Proton Therapy in the Treatment of Lung Cancers. Cancer J 2014;20:427–32.
[4] Baumann BC, et al. Comparative Effectiveness of Proton vs Photon Therapy as Part of concurrent Chemoradiotherapy for locally Advanced Cancer. JAMA Oncol 2020;6:237.
[5] Gabani P, et al. Clinical outcomes and toxicity of proton beam radiation therapy for re-irradiation of locally recurrent breast cancer. Clin Transl Radiat Oncol 2019;19:116–22.
[6] Newhauser WD, Zhang R. The physics of proton therapy. Phys Med Biol 2015;60:R155–209.
[7] Lomax AJ, et al. Intensity modulated proton therapy: a clinical example. Med Phys 2001;28:317–24.
[8] Lomax A. Intensity modulation methods for proton radiotherapy. Phys Med Biol 1999;44:185–205.
[9] Smith AR. Vision : Proton therapy. Med Phys 2009;36:556–68.
[10] the evolution of ultra-precise proton therapy. Choi, J. I., Hasan, S., Press, R. H., Chhabra, A. M. & Simone Ii, C. B. Sharpening the particle knife. Ther Radiol Oncol 2021;5:3.
[11] Kooy HM, et al. A Case Study in Proton Pencil-Beam Scanning delivery. Int J Radiat Oncol 2010;76:624–30.
[12] Depuydt T. Proton therapy technology evolution in the clinic: impact on radiation protection. Ann ICRP 2018;47:177–86.
[13] Grosshans DR, et al. Spot Scanning Proton Therapy for Malignancies of the Base of Skull: Treatment Planning, Acute Toxicities, and Preliminary Clinical Outcomes. Int J Radiat Oncol 2014;90:540–6.
[14] Kase Y, et al. A Treatment Planning Comparison of Passive-Scattering and Intensity-Modulated Proton Therapy for typical Tumor Sites. J Radiat Res (Tokyo) 2012;53:272–80.
[15] Zhu L, Zhang M, Xiang X, Wang X. Dose-Area Product Determination and Beam Monitor Calibration for the Fixed Beam of the Shanghai Advanced Proton Therapy Facility. Appl Sci 2022;12:4111.
[16] Palmans H, Vatnitsky SM. Beam monitor calibration in scanned light-ion beams. Med Phys 2016;43:5835–47.
[17] Karger CP, Jäkel O, Palmans H, Kanai T. Dosimetry for ion beam radiotherapy. Phys Med Biol 2010;55:R193–234.
[18] Gomà C, Safai S, Vörös S. Reference dosimetry of proton pencil beams based on dose-area product: a proof of concept. Phys Med Biol 2017;62:4991–5005.
[19] International atomic energy agency. *Absorbed Dose Determination in External Beam Radiotherapy*. (INTERNATIONAL ATOMIC ENERGY AGENCY 2024. https://doi.org/10.61092/iaea.ve7q-y94k.
[20] Tan HQ, et al. The effect of spill change on reliable absolute dosimetry in a synchrotron proton spot scanning system. Med Phys 2023;50:4067–78.
[21] Peterson S, et al. Variations in proton scanned beam dose delivery due to uncertainties in magnetic beam steering: Proton dose variations from magnetic steering uncertainties. Med Phys 2009;36:3693–702.
[22] Yu J, Beltran CJ, Herman MG. Implication of spot position error on plan quality and patient safety in pencil-beam-scanning proton therapy. Med Phys 2014;41:081706.
[23] Rana S, Rosenfeld AB. Impact of errors in spot size and spot position in robustly optimized pencil beam scanning proton-based stereotactic body radiation therapy (SBRT) lung plans. J Appl Clin Med Phys 2021;22:147–54.
[24] Arjomandy B, et al. AAPM task group 224: Comprehensive proton therapy machine quality assurance. Med Phys 2019;46.
[25] Osorio J, et al. Beam monitor calibration of a synchrotron-based scanned light-ion beam delivery system. Z Für Med Phys 2021;31:154–65.
[26] Tan HQ, et al. Denoising proton reference dosimetry spectrum using a large area ionization chamber—physical basis and type a uncertainty. Phys Med Biol 2025;70:025003.
[27] Green S, et al. IPEM code of practice for proton therapy dosimetry based on the NPL primary standard proton calorimeter calibration service. Phys Med Biol 2025;70:065016.